

Exchange Correlation Potentials from Full Configuration Interaction in a Slater Orbital Basis

Soumi Tribedi,^{1,2} Duy-Khoi Dang,¹ Bikash Kanungo,³ Vikram Gavini,^{3,4} and Paul M. Zimmerman^{1, a)}

¹⁾*Department of Chemistry, University of Michigan, Ann Arbor, Michigan 48109, United States*

²⁾*Michigan Institute for Data Science, University of Michigan, Ann Arbor, Michigan 48109, United States*

³⁾*Department of Mechanical Engineering, University of Michigan, Ann Arbor, Michigan 48109, United States*

⁴⁾*Department of Materials Science and Engineering, University of Michigan, Ann Arbor, Michigan 48109, United States*

(Dated: 1 August 2024)

RKS theory builds a bridge between wave function theory and density functional theory by using quantities from the former to produce accurate exchange-correlation potentials needed by the latter. In this work, the RKS method is developed and tested alongside Slater atomic orbital basis functions for the first time. To evaluate this approach, Full Configuration Interaction computations in the Slater orbital basis are employed to give quality input to RKS, allowing full correlation to be present along with correct nuclei cusps and asymptotic decay of the wavefunction. SlaterRKS is shown to be an efficient algorithm to arrive at exchange correlation potentials without unphysical artifacts in moderately-sized basis sets. Furthermore, enforcement of the nuclear cusp conditions will be shown to be vital for the success of the Slater-basis RKS method. Examples of weakly and strongly correlated molecular systems will demonstrate the main features of SlaterRKS.

I. INTRODUCTION

Density Functional Theory (DFT)¹⁻³, particularly within the Kohn Sham (KS) formalism,⁴ provides a cost-effective, scalable means for approximating the quantum behavior of electronic states. The KS equations are

$$\left[-\frac{1}{2}\nabla^2 + v(\mathbf{r}) + v_H(\mathbf{r}) + v_{XC}(\mathbf{r}) \right] \phi_i(\mathbf{r}) = \varepsilon_i \phi_i(\mathbf{r}), \quad (1)$$

and ϕ_i are the KS orbitals, which together comprise a system of non-interacting electrons having the density $\rho^{KS}(\mathbf{r}) = \sum_i n_i |\phi_i(\mathbf{r})|^2$.⁵ The orbital energies, ε_i , arise from the kinetic energy and three potentials: $v(\mathbf{r})$ is the external potential (usually the nuclear potential), $v_H(\mathbf{r})$ is the Hartree potential which accounts for the classical Coulomb interaction between electrons, and $v_{XC}(\mathbf{r})$ is the exchange-correlation potential which contains the non-classical contribution from the kinetic energy and electron-electron repulsion. The unknown component of DFT, $v_{XC}(\mathbf{r})$, is defined as the functional derivative of the XC energy functional,

$$v_{XC}(\mathbf{r}) = \frac{\delta E_{XC}[\rho(\mathbf{r})]}{\delta \rho(\mathbf{r})}. \quad (2)$$

The functional of the density, $E_{XC}[\rho(\mathbf{r})]$, and its derivative in Eq. 2 are approximated in practice. Together, Eqs. 1 and 2 are used to solve for KS orbitals, which provide a description of the electron density and its corresponding energy.

The choice of the approximate form for $E_{XC}[\rho(\mathbf{r})]$ is made from the various rungs of the 'Jacob's Ladder' of functionals that have been developed over the past half century.⁶ The

capabilities of DFT for molecules⁷⁻⁹ and solids¹⁰⁻¹² have undoubtedly increased over this time, but questions still remain regarding well-documented problems with self-interaction, delocalization errors, and strong correlation.¹³⁻¹⁶ Since these errors are tied closely to the electron density, it is clear that improvements to $v_{XC}(\mathbf{r})$ are needed to improve upon current DFT approximations.

The focus of this article is therefore on the exchange-correlation potential, since knowledge about this potential could lead to improved functional approximations.¹⁷⁻²¹ This point has been emphasized by recent work showing that widely used functionals give rise to potentials that are far from the exact (even for SCAN0 which has v_{XC} closest to the exact, the errors are in the range of $O(10^{-1} - 10^0)$).²² These errors may be attributed to the standard practice of functional training to reproduce energies, while neglecting errors in the exchange-correlation potential. Providing this information, however, requires means to accurately compute $v_{XC}(\mathbf{r})$, which is a highly nontrivial task.

For a given reference density, the corresponding XC potential can in principle be obtained numerically by the inverse DFT approach.²³ The inverse problem maps a given density to its corresponding potential through a unique one-to-one mapping.^{4,24} The inverse relation, however, is well posed only in a complete basis.^{25,26} In an incomplete basis the unique mapping of potential to density does not hold true, i.e., different XC potentials can map to the same density.²⁷⁻²⁹ In practice, inverse calculations are often performed using incomplete basis sets (such as finite Gaussian basis sets) and persistent numerical problems result. Recently, Kanungo et al. implemented a complete, finite-element basis and used it to obtain highly accurate potentials,³⁰ and Stücker et al. alleviated the problem using a multiresolution wavelet basis to similar effect.³¹ These recent results show the possibilities of complete basis sets in tackling the inverse DFT problem, but have not improved upon the situation for finite basis sets.

^{a)}Electronic mail: paulzim@umich.edu

Elegantly skipping past the inverse DFT problem, Staroverov and coworkers developed means to obtain $v_{XC}(\mathbf{r})$ from the reduced density matrices (RDMs) of any wavefunction method.^{32,33} The RKS method evaluates $v_{XC}(\mathbf{r})$ from the comparison of two local energy balance equations, one originating from the KS equations and the other from wavefunction theory. Since the RKS method uses the wavefunction instead of the density to obtain the potential and employs systematic approximations to the kinetic energy density, it is free from the stringent requirements of basis set completeness that plague inversion techniques.³⁴ Using RKS, potentials can be straightforwardly derived for atoms and molecules in moderate or larger Gaussian basis sets. Even though densities expanded in Gaussian type orbitals (GTOs) have inherent shortcomings, the stability of the RKS (and mRKS) methods in obtaining accurate exchange-correlation potentials is a promising step forward for finite-basis DFT. To go further with the RKS method, we envisioned improving the wave function, electron densities, and $v_{XC}(\mathbf{r})$ by the use of Slater type orbitals (STO).³⁵

STOs have good physical properties that are expected for electronic states, for instance the ability to describe cusps at the nuclei and at long range, exponentially decaying tails.^{36–38} Particularly in the construction of densities and the corresponding potentials, these properties make STOs a better choice than GTOs, which suffer from unphysical oscillatory behaviour under the Laplacian.³⁵ While STOs have seen less use than GTOs in quantum chemistry, their limitations can be traced to the difficult two-electron integral evaluation, which must be done numerically in 6 dimensions. Recently Zimmerman and coworkers developed an efficient GPU-accelerated algorithm to evaluate STO integrals in the resolution-of-the-identity (RI) approximation.³⁹ This opened up the opportunity for us to carry out the RKS procedure with STO basis sets.

By using STO basis sets, one important property of the electron density can be naturally incorporated into the RKS procedure. The Kato cusp condition specifies how the density must behave near the nucleus.³⁶ This condition is met when every occupied molecular orbital satisfies

$$\left. \frac{\partial \phi_i}{\partial \mathbf{r}} \right|_{\mathbf{r}=R_B} = -Z_B \phi_i(R_B), \quad (3)$$

where R_B is the position of a nucleus B with atomic number Z_B . With STOs, the cusp condition can be enforced by using a modified SCF procedure⁴⁰ which will be described in the Methods section. As a result, the singularity due to electron-nuclear attraction at the nucleus will be compensated by the kinetic energy. This property appears unreachable in finite GTO basis sets, and its effect on $v_{XC}(\mathbf{r})$ near the nucleus will be an interesting question to examine (Section IV).

This article presents exchange correlation potentials for atoms and molecules, derived from highly accurate full configuration interaction (FCI) densities using Slater type orbitals. FCI wave functions in STO basis sets capture all dynamic and static correlation available to the basis, with the additional benefit of having the correct nuclear cusp and long range asymptotic behavior. The ability to calculate XC potentials at this high level of theory will therefore be examined for the first time in the results that follow.

II. METHOD

The RKS method utilizes the one particle and two particle reduced density matrices (1-RDM and 2-RDM respectively) of the wavefunction to evaluate v_{XC} .³² The notations WF or KS are used throughout this manuscript to denote the terms derived from wavefunction or KS-DFT methods, respectively. The RKS working equation,

$$v_{XC}(\mathbf{r}) = v_S^{WF}(\mathbf{r}) + \frac{\tau^{WF}(\mathbf{r})}{\rho^{WF}(\mathbf{r})} - \frac{\tau^{KS}(\mathbf{r})}{\rho^{KS}(\mathbf{r})} + \epsilon^{KS}(\mathbf{r}) - \epsilon^{WF}(\mathbf{r}), \quad (4)$$

is derived from local energy balance equations under the condition $\rho^{WF}(\mathbf{r}) = \rho^{KS}(\mathbf{r})$. Here, $\rho^{WF}(\mathbf{r})$ is fixed to that of the wavefunction reference, and $\rho^{KS}(\mathbf{r})$ is the density from the self-consistent solutions of the KS equations (Eq. 1). The Slater exchange-correlation charge potential, $v_S^{WF}(\mathbf{r})$,⁴¹ is expressed as,

$$v_S^{WF}(\mathbf{r}) = \int \frac{\rho_{XC}^{WF}(\mathbf{r}, \mathbf{r}_2)}{|\mathbf{r} - \mathbf{r}_2|} d\mathbf{r}_2, \quad (5)$$

where, $\rho_{XC}^{WF}(\mathbf{r})$ is the exchange-correlation hole density derived from the relation, $\Gamma(\mathbf{r}, \mathbf{r}_2; \mathbf{r}, \mathbf{r}_2) = P(\mathbf{r}, \mathbf{r}_2) = \frac{1}{2} \rho^{WF}(\mathbf{r}) [\rho^{WF}(\mathbf{r}_2) + \rho_{XC}^{WF}(\mathbf{r}, \mathbf{r}_2)]$. The positive-definite kinetic energy densities, $\tau(\mathbf{r})$, and the average local electron energies, $\epsilon(\mathbf{r})$, are defined as,

$$\tau^{WF}(\mathbf{r}) = \frac{1}{2} \sum_i n_i |\nabla \psi_i(\mathbf{r})|^2, \quad (6)$$

$$\tau^{KS}(\mathbf{r}) = \frac{1}{2} \sum_i n_i |\nabla \phi_i(\mathbf{r})|^2, \quad (7)$$

$$\epsilon^{WF}(\mathbf{r}) = \frac{1}{\rho^{WF}(\mathbf{r})} \sum_j \lambda_j |\psi_j(\mathbf{r})|^2, \quad (8)$$

$$\epsilon^{KS}(\mathbf{r}) = \frac{2}{\rho^{KS}(\mathbf{r})} \sum_{i=1}^{N/2} \epsilon_i |\phi_i(\mathbf{r})|^2, \quad (9)$$

where the orbitals ψ_j are associated with generalized Fock eigenvalues λ_j , and ϕ_i are the set of KS orbitals with eigenvalues ϵ_i . Other choices for the kinetic energy densities are the Laplacian and Pauli forms. In the original RKS method, the positive-definite kinetic energy was used rather than the Laplacian kinetic energy ($\tau_L^{KS} = -\frac{1}{2} \sum_i n_i \phi_i^*(\mathbf{r}) \nabla^2 \phi_i(\mathbf{r})$) which are related by $\tau_L = \tau - 0.25 \nabla^2 \rho$.^{32,33} This choice can be motivated by equating KS and WF densities (i.e. $\rho^{KS} = \rho^{WF}$) or by observing that the positive-definite kinetic energy is more numerically stable near an atom. In the modified RKS method, the Pauli kinetic energy density ($\tau_P = \tau - |\nabla \rho|^2 / 8\rho$)⁴² is used to proceed further along this path. For Slater-based RKS, two forms of kinetic energy densities were evaluated (Laplacian and positive definite), and it was found that the positive definite form has better properties (vide infra).

The above RKS equations give $v_{XC}(\mathbf{r})$ up to an arbitrary constant. At the asymptotic limit of $\mathbf{r} \rightarrow \infty$, $v_{XC}(\mathbf{r}) \rightarrow v_S^{WF}(\mathbf{r}) \sim -1/\mathbf{r}$. ϵ^{KS} and $-\tau^{KS}/\rho^{KS}$ approach ϵ_{HOMO} , whereas the analogous wavefunction terms approach $-I_{min}$, the first ionization energy from extended Koopman's theorem. In order to enforce the asymptotic decay of $v_{XC}(\mathbf{r})$ (and determine the constant), all the terms to the right of Eq. 4 except for the v_S^{WF} must cancel at $\mathbf{r} \rightarrow \infty$. Therefore all the eigenvalues of the KS orbitals are shifted such that $\epsilon_{HOMO} = -I_{min}$ is satisfied. Further, in the far field, where the densities are almost zero, the numerical evaluation of the kinetic energy densities, i.e. the second and third terms in Eq. 4 yields unphysically large values. Since at large distances v_{XC} and v_S^{WF} are expected to be identical, a function (F) is used to smoothly transition v_{XC} into v_S^{WF} at the threshold of low density ($\theta = 10^{-5}$),

$$v_{XC}(\mathbf{r})^{smooth} = F(\mathbf{r})v_{XC}(\mathbf{r}) + (1 - F(\mathbf{r}))v_S^{WF}(\mathbf{r}) \quad (10)$$

where,

$$F(\mathbf{r}) = \frac{\rho(\mathbf{r})}{\rho(\mathbf{r}) + \theta} \quad (11)$$

The algorithm of the RKS method (Fig. 1) entails evaluating the wavefunction terms first, i.e., $v_S^{WF}(\mathbf{r})$, $\rho^{WF}(\mathbf{r})$, $\tau^{WF}(\mathbf{r})$, and $\epsilon^{WF}(\mathbf{r})$. Next, an initial guess for the KS orbitals is chosen and the corresponding terms, $\rho^{KS}(\mathbf{r})$, $\tau^{KS}(\mathbf{r})$ and $\epsilon^{KS}(\mathbf{r})$ are evaluated and the ϵ_i are shifted with respect to I_{min} . Eq. 4 then provides $v_{XC}(\mathbf{r})$. This potential is then used to solve for new KS orbitals from Eq. 1, and the KS terms are updated in Eq. 4 until $v_{XC}(\mathbf{r})$ and the KS orbitals become self-consistent.

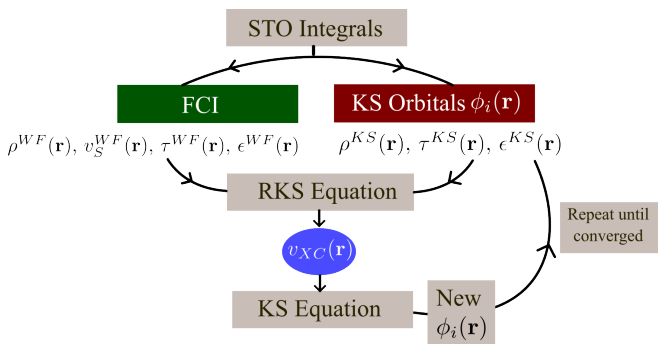


FIG. 1. The algorithm of the RKS method using STO integrals

In all, the SlaterRKS procedure follows the original RKS procedure that used a Gaussian basis set, except for a few details. In particular, it is notable that due to the correct short- and long-range behavior of Slater orbitals, the Laplacian kinetic energy operator, $\tau_L^{KS}(\mathbf{r})$ may be a tractable choice. This will be the case only when the conditions of the next paragraph are under consideration.

The molecular orbitals used for the WF and KS theories are constrained to obey Kato's cusp condition (Eq. 3) using Handy's method.⁴⁰ Each molecular orbital is expanded in terms of the basis functions (χ), i.e. $\phi_i = \sum_{\alpha A} c_{\alpha A, i} \chi_{\alpha A}$, where the sum is over exponent α and the atom A on which the basis

functions are centered, and c_i are the MO coefficients corresponding to the i^{th} MO. Kato's condition gives

$$\sum_{\alpha A} p_{\alpha A, BC} c_{\alpha A, i} = 0, \quad (12)$$

where,

$$p_{\alpha A, B} = \left. \frac{\partial \chi_{\alpha B}}{\partial \mathbf{r}_B} \right|_{\mathbf{r}_B=0} \delta_{AB} + Z_B \chi_{\alpha A}(\mathbf{r}_B) \quad (13)$$

The condition of Eq. 12 is enforced by using a modified SCF procedure with,

$$[(\mathbf{I} - \mathbf{A})(\mathbf{F} - \epsilon \mathbf{S})(\mathbf{I} - \mathbf{A})] \mathbf{c} = 0, \quad (14)$$

where $\mathbf{A} = \sum_{BC} \hat{\mathbf{p}}_B (\hat{\mathbf{p}}_B^T \hat{\mathbf{p}}_C)^{-1} \hat{\mathbf{p}}_C^T$. This procedure ensures that all MOs in the correlated wavefunction have correct electron-nuclear cusps, and the same will be true when solving the KS equations.

III. COMPUTATIONAL DETAILS

The SlaterRKS method was implemented in C++ and interfaced with the SlaterGPU³⁹ library to evaluate integrals for Slater basis functions using GPU acceleration. All Coulomb integrals will therefore be evaluated using the Resolution of the Identity (RI) approximation.⁴³⁻⁴⁵ The orbitals and RDMs for the reference WFs come from the heat-bath configuration interaction (HBCI) procedure⁴⁶⁻⁵⁰ using a tight threshold (He, H₂, LiH: 10^{-5} Ha and H₂O, CH₂: 10^{-4} Ha) for accuracy of the variational wavefunction. For atoms and small molecules, the RDMs from this approach will be essentially FCI quality.

The primary working equation in the SlaterRKS method is Eq. 4, where all the quantities are evaluated according to their expressions given in Eqs 5-9. Evaluation of these equations is accelerated on GPU using OpenACC to generate their contribution to v_{XC} on the grid. For Eqs 6-9, a simple `acc parallel` directive is prepended to each for-loop over the grid points. Evaluation of $v_S^{WF}(\mathbf{r})$ via Eq. 5 is the most expensive step due to the 6-dimensional integration over two electrons. To minimize wall-time, OpenMP and OpenACC are jointly used to compute $v_S^{WF}(\mathbf{r})$. Therefore, contributions from Eq. 5 involve two nested for-loops, each over the entire grid. The outer for-loop is parallelized with OpenMP where one thread is launched for each GPU. The inner for-loop is then parallelized with OpenACC using the `acc parallel` directive with a `reduction` clause. The `reduction` clause indicates a summation in the inner for-loop, which reflects the numerical evaluation of the integral in Eq. 5. Since the same grid and integral weights are used for each inner for-loop, they only need to be generated once before entering the outer for-loop of Eq. 5.

The Slater basis sets were taken from the set developed by Baerends and coworkers.⁵¹ Four types of basis set are included in this set, namely DZP, TZP, TZ2P and QZ4P. The DZP, TZP and TZ2P basis sets have double zeta-core functions, while the QZ4P has a triple-zeta core. In the valence region, the DZ is double zeta, TZP and TZ2P triple zeta, and

QZ4P quadruple zeta, all with valence polarization functions. For example, the QZ4P basis has $3 \times 1s$, $4 \times 2s$, $4 \times 2p$, $2 \times 3d$ and $2 \times 4f$ functions for C atom. Larger basis sets were needed to test the cusp condition implementation on the helium atom (vide infra). 5Z6P and 6Z6P basis sets were thus created in an even-tempered manner, following the procedure of Baerends and coworkers⁵² (see Supporting Information for full specification of these basis sets).

The geometries and ionization energies (I_{min}) are taken from the CCCBDB database⁵³ and provided in the Supporting Information. The STO integral evaluation as well as the RKS procedure is carried out on numerical atom-centered grid.⁵⁴⁻⁵⁶ The three dimensional grid is composed of products of radial⁵⁵ and angular⁵⁷ points with weights according to the Becke partitioning scheme.⁵⁴ In all the calculations in this manuscript, 50 radial and 5810 angular points are employed for each atom.

The convergence of each SlaterRKS run is verified by the L_1 and L_2 errors in the KS density compared to the reference WF. The norms, ΔX_{L_1} and ΔX_{L_2} of a property X are defined as,

$$\Delta X_{L_1} = \int |X^A(\mathbf{r}) - X^B(\mathbf{r})| d\mathbf{r} \quad (15)$$

$$\Delta X_{L_2} = \sqrt{\int (X^A(\mathbf{r}) - X^B(\mathbf{r}))^2 d\mathbf{r}} \quad (16)$$

where A and B are the reference and calculated values. The calculation is deemed converged when the $\Delta\rho_{L_1}$ does not change more than 10^{-5} from one iteration to the next.

IV. RESULTS AND DISCUSSION

In this section the SlaterRKS method is applied to a few prototypical test systems along with a few strongly correlated test cases. The simplest example is the two electron case of hydrogen molecule at three separate bond distances—equilibrium, twice the equilibrium and fully dissociated. The next example is the heteronuclear LiH molecule. In addition the water molecule is examined as a small polyatomic, followed by the more challenging multireference test case of singlet methylene (CH_2). For all of these examples, FCI wavefunctions in the Slater orbital basis sets will be used (unless otherwise noted) as the reference for the RKS procedure.

Before delineating these examples, it is emphasized that the enforcement of the long-range asymptotic behavior is important to reach meaningful exchange correlation potentials. The correct asymptotic decay of v_{XC} follows $-1/r$,^{58,59} though LDA and GGA functionals fail to satisfy this condition.⁶⁰ Properties such as the energy of the HOMO, which is tied closely to the ionization energy, will only be accurate with correct asymptotics.⁶¹ In the RKS method, this condition is enforced by shifting v_{XC} such that $\epsilon_{HOMO} = -I_{min}$. In SlaterRKS, an additional condition (see method section) ensures a smooth transition $v_{XC}(\mathbf{r}) \rightarrow v_S^{WF}(\mathbf{r})$ as $r \rightarrow \infty$. The Supporting

Information shows the $\text{H}_2(\text{eq.})$ molecule, where v_{XC} and v_S^{WF} decay as $-1/r$ at low density regions far from the nuclei.

While the cusp condition (Eq. 3) will be applied for most of the SlaterRKS results of this work, it will first be evaluated for the helium atom in a range of basis sets. Numerical evaluation of Kato's equation on a few grid points near the nucleus is shown in Tables S2-S5 in the SI. These results confirm the cusp enforcement reduces the error at $\mathbf{r} = 10^{-6}$ (i.e. at the nuclear position) by two orders of magnitude or more compared to densities without the cusp condition. Obtaining this accuracy near the nucleus, however, is not free because one degree of freedom per atom is lost in the basis when the constraint is applied. Therefore the dependence of the SlaterRKS results on the basis set size needs to be examined before applying the cusp condition more widely.

Fig. 2 shows the L_1 error of density from the SlaterRKS procedure (blue) and the corresponding FCI correlation energy (E_{corr}) (red) with cusp condition (solid line) and without (dashed line) for the helium atom. With increase in basis set size, the correlation energy improves systematically and converges. In all basis sets, the E_{corr} is lower when the cusp condition is enforced. In the smaller TZ2P basis set this effect is quite significant, resulting in a 5 mHa decrease in correlation energy at the FCI level. The effect diminishes to the sub-mHa level with larger basis sets (QZP and higher). The errors in the KS density (compared to the WF reference) behave similarly. With larger basis sets, the L_1 errors for the pairs of densities agree within $O(10^{-4})$ a.u. and converge to a common point (see Table S6 in the supporting information). Differences remain in L_1 errors between the cusp-enforced vs. cusp-not-enforced densities at the TZ2P level, reflecting the smallness of this basis. For the larger basis set sizes, the cusp condition can readily be applied, giving an improved description of the density at the nucleus.

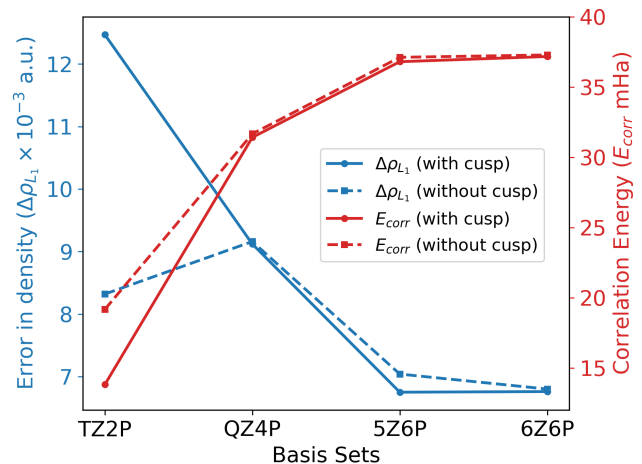


FIG. 2. Results for He atom in various basis sets. Left-hand axis: Comparison of L_1 errors of RKS densities with respect to CI densities when the cusp condition is applied vs. not applied. Right-hand axis: Correlation energies.

Having established how the SlaterRKS procedure behaves

with and without a cusp condition, the next item to examine is the effect of basis set size, this time in a diatomic molecule. Results for the H_2 molecule (at its equilibrium geometry) with various basis sets are therefore shown in Fig. 3. The DZP basis set is too small to be meaningfully used alongside the cusp condition, but the others include the Kato cusp. Far from the nuclei where the density is low, the three different basis sets result in similar potentials. As more correlation is present near the bonding region, the larger basis sets (TZ, QZ) produce deeper wells in the exchange correlation potential, though the three basis sets give qualitatively similar structures consisting of double-well potentials. For comparison, the SlaterRKS potential from the HF wavefunction is also shown in Fig. 3. Notably, v_{XC} from HF is missing the characteristic maximum in the middle of the bond, due to the lack of electron correlation.

Fig. 4 shows the differences in density between FCI and SlaterRKS for the QZ4P, TZ2P and DZP basis sets. The corresponding L_1 and L_2 errors in the density for these calculations are given in the Supporting Information. As reflected in the original RKS procedure in a Gaussian basis, larger basis sets do a better job at reproducing WF electron densities.^{32,33} The Laplacian kinetic energy (τ_L) can also be used in place of the positive-definite form, which is shown for the QZ4P basis set (see Supporting Information). The sharp features in the $\tau_L - v_{XC}$ are due to the divergence of the Laplacian near the nucleus, which arise due to the differences in WF and KS KE density via Eq. 4. In all, because the larger (QZ4P) Slater basis set and positive-definite KE operator produced the best density (as well as potential), the remaining SlaterRKS results in this work were carried out using the QZ4P basis set, FCI RDM, and the positive-definite KE operator.

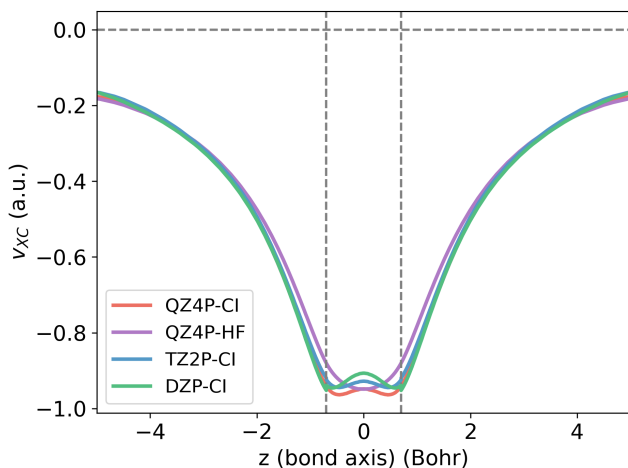


FIG. 3. The exchange correlation potential of H_2 (eq.) along the bond axis calculated using different basis sets and theoretical method. $v_{XC} = 0$ is shown as a horizontal grey dashed line.

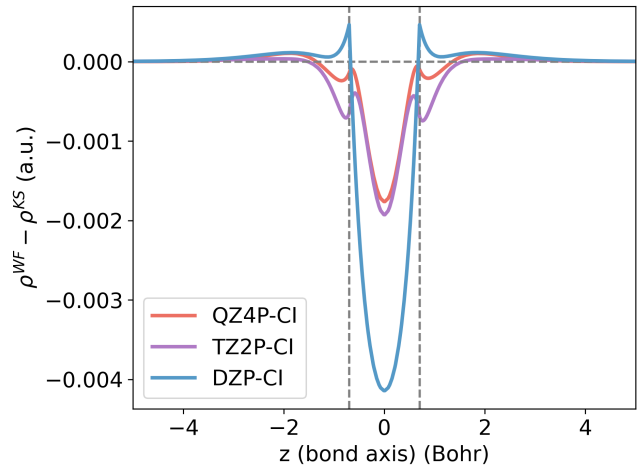


FIG. 4. The difference in the FCI and RKS densities for H_2 (eq.) along the bond axis. $\rho^{WF} - \rho^{KS} = 0$ is shown as a horizontal grey dashed line.

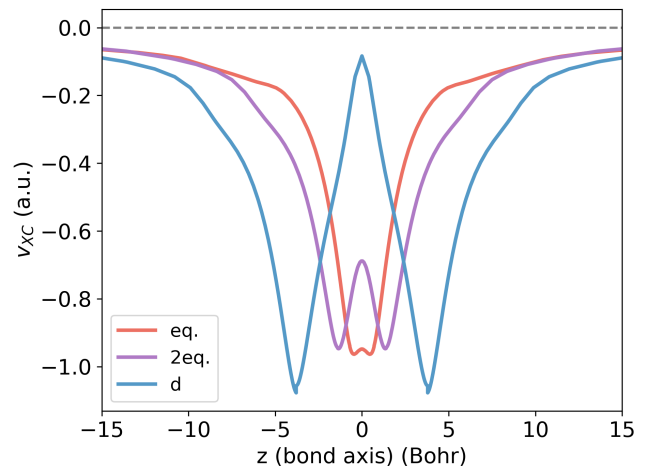


FIG. 5. The exchange correlation potential of H_2 along the bond axis with the hydrogen atoms spaced at 1.4010 a.u. (equilibrium distance) in red, 2.8020 a.u. ($2 \times$ equilibrium distance) in purple, and 7.58 a.u. (dissociation bond length) in blue. $v_{XC} = 0$ is shown as a horizontal grey dashed line.

TABLE I. Normalized L_1 errors and L_2 errors of density from RKS with respect to CI densities in the QZ4P basis set

| System | $\Delta\rho_{L_1}/N_e$ | $\Delta\rho_{L_2}$ |
|--------------|------------------------|-----------------------|
| H_2 (eq.) | 4.06×10^{-3} | 1.58×10^{-3} |
| H_2 (2eq.) | 1.37×10^{-2} | 3.70×10^{-3} |
| H_2 (d) | 8.86×10^{-3} | 1.49×10^{-3} |
| LiH | 4.66×10^{-3} | 4.68×10^{-3} |
| CH_2 | 4.91×10^{-3} | 8.33×10^{-3} |
| H_2O | 3.28×10^{-3} | 1.88×10^{-2} |

To show the behavior of SlaterRKS as strong correlation is

introduced to the reference WF, three geometries of the H_2 molecule were examined. The L_1 errors of densities normalized by the number of electrons ($\Delta\rho_{L_1}/N_e$) are given in Table I for the QZ4P basis set. Excellent agreement of the RKS and FCI densities in the case of the equilibrium geometry of H_2 is demonstrated by the normalized L_1 error in the order of 10^{-3} . The increase in the L_1 errors at the elongated bond lengths is expected as strong correlation increases. The features of the v_{XC} s (shown along the H–H bond in Fig. 5) are largely representative of the exact potentials obtained using the finite-element inverse calculation.²² For the strongly correlated cases of stretched H_2 molecules, where most functionals fail, the SlaterRKS potentials are promising. The depth of the potential at the nucleus and the height of the maxima between the nuclei gradually increase as the bond length increases, signifying gradual depletion of electron density between the bond.

Moving on to a diatomic with more electrons, SlaterRKS analysis for the minimum energy geometry of LiH is shown in Fig. 6. Various commonly used DFT XC potentials have a deeper well at Li, whereas the SlaterRKS v_{XC} is shallower, closer to the accurate finite-element inverse calculation.²² To the left of the Li potential well, an intershell feature is present, typical of accurate v_{XC} s. The largest errors in the density are near the Li nucleus (Fig. 6 inset). This is likely the case because the QZ4P basis has only three core (1s) atomic orbitals, limiting the ability of SlaterRKS to resolve the density to higher accuracy. Regardless, the L_1 errors in the density are still relatively low, as reflected in Table I, and still might be improved with the availability of larger Slater basis sets.

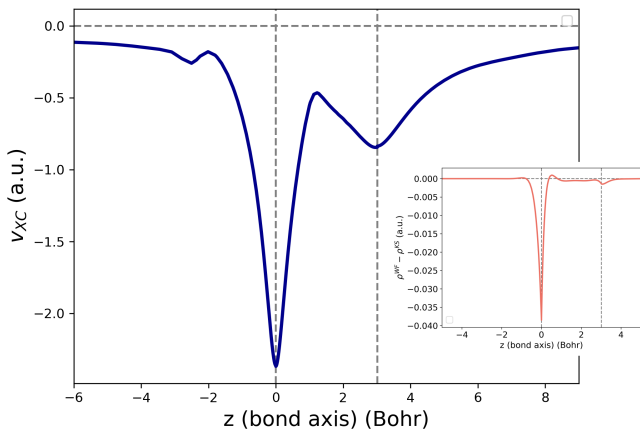


FIG. 6. The exchange correlation potential of LiH along the bond axis at the equilibrium separation of 3.01392 a.u. The vertical dashed lines represent the position of each nuclei. The difference in densities $\rho^{WF} - \rho^{KS}$ is plotted in the inset.

The polyatomic H_2O molecule was next subjected to SlaterRKS analysis. The v_{XC} shown in Fig. 7 along one of the O–H bonds also has the distinctive intershell structure near the oxygen. There is no discernible minimum at the H nucleus—only a change in curvature—due to the dominance of the oxygen atom’s potential in this region. The potential well at oxygen

is less deep than that seen with the finite-element potential,²² suggesting a smaller exchange-correlation effect at that position in the SlaterRKS case. The two dimensional plot of v_{XC} in the plane of the molecule is shown in Fig. 8. As with prior studies in the complete basis set, inverse DFT limit, the inter-shell feature around the O atom is discernible from the orange ring around the darker O nucleus. This feature is typically absent in conventional DFT functionals.²²

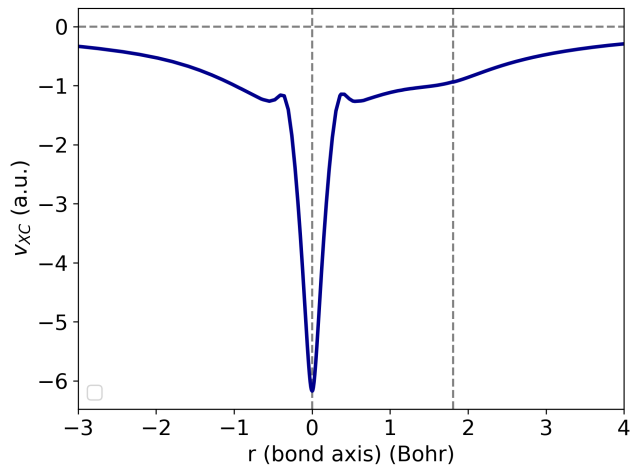


FIG. 7. The exchange correlation potential of H_2O along the bond axis of one of the O–H bonds. The O atom is at 0 a.u. and the H is at 1.81 a.u. The vertical dashed lines represent the position of each nuclei.

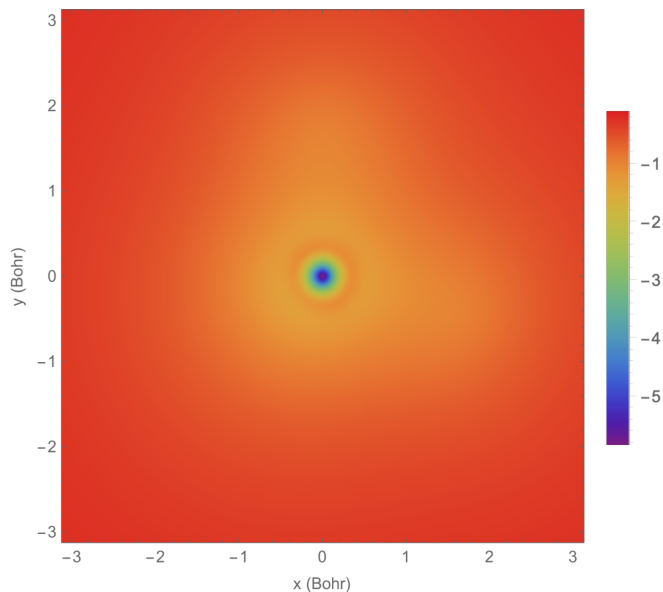


FIG. 8. The exchange correlation potential of H_2O in the plane of the molecule.

The importance of having correct nuclear cusps was emphasized in the introduction, and an explicit enforcement of these cusps is present in the SlaterRKS algorithm. The H_2O

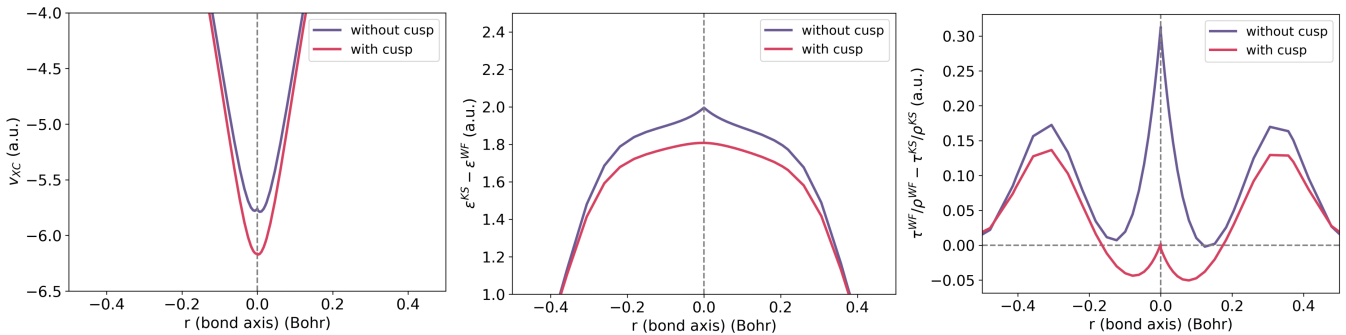


FIG. 9. The v_{XC} , $\epsilon^{KS} - \epsilon^{WF}$ and $\tau^{WF}/\rho^{WF} - \tau^{KS}/\rho^{KS}$ for H_2O zoomed in to $\mathbf{r} = 0$ (O atom) position to demonstrate the effect of the cusp condition.

molecule provides a good example to demonstrate the nature of SlaterRKS v_{XC} with and without the cusp condition being enforced (Eq. 3). Fig. 9 shows v_{XC} in a small region around the oxygen nucleus. The peak that forms without the cusp condition is unexpected, and likely an artifact of using Slater orbitals that have steep slopes near the nucleus (see Eq. 7). Since Gaussian orbitals have zero slope at the nucleus, such behavior is less likely with finite-sized Gaussian basis sets. Fortunately, enforcement of the nuclear cusp condition dramatically remedies this situation, producing a more physical, single well potential near the oxygen nucleus. The middle and right side of Fig. 9 show that the better behavior in the cusp-enforced case stems from smoother contributions to v_{XC} from ϵ and τ , since the Slater potentials are monotonic (see SI). The contributions from ϵ and τ without the cusp condition have more features—which do not cancel out—and overall result in a significant, likely incorrect effect on v_{XC} .

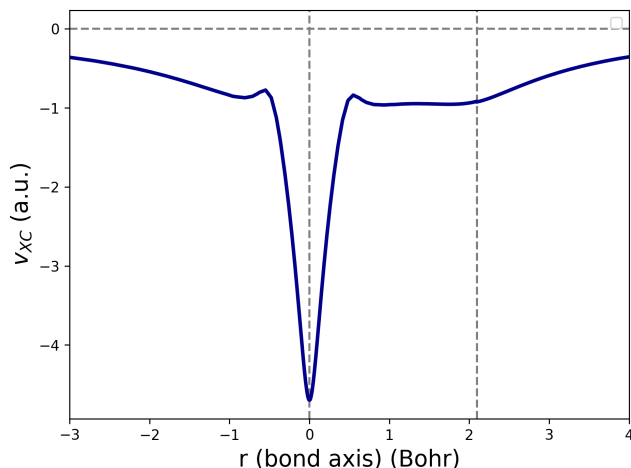


FIG. 10. The exchange correlation potential of CH_2 along the bond axis of one of the C–H bonds. The C atom is at 0 a.u. and the H is at 2.0955 a.u. The vertical dashed lines represent the position of each nuclei.

Finally, SlaterRKS is used to examine a strongly correlated polyatomic. The lowest energy singlet state (1A_1) of the CH_2

(methylene) molecule has significant contributions from two electron configurations,

$$(1a_1)^2(2a_1)^2(1b_2)^2(3a_1)^2$$

and,

$$(1a_1)^2(2a_1)^2(1b_2)^2(1b_1)^2$$

giving this state a multiconfigurational nature.^{50,62,63} Fig. 10 shows the SlaterRKS XC potential along one of the C–H bonds. The depth of the potential at the carbon nucleus is -4.7 a.u. which is in good agreement to previous reports.^{64,65} The intershell structure distinguishing the core and valence regions around the C atom is also present, as expected. The potential at the H nucleus resembles the trailing valence region of the C atom, similar to the H_2O situation. The nature of the v_{XC} in the bonding region of the C–H bond of CH_2 is more flat than that in O–H, which is a characteristic feature of less ionic covalent bonds.⁶⁶

The potential from Fig. 10 results in an L_1 error in the electron density of $O(10^{-3})$, which is a satisfactory result given the complexity of the reference WF, which is from complete CI computations in the QZ4P basis set. The CI result includes population of 0.05958 electrons in the p orbital, a significant amount that is difficult to capture in the pure-state KS representation of the density. While this example has not been studied before using RKS theory, the SlaterRKS method appears up to the task of treating strong correlation in the challenging CH_2 molecule.

V. CONCLUSIONS

This work found that RKS theory using a Slater basis set is a useful tool for examining exchange-correlation potentials corresponding to FCI wavefunctions. Features of the potentials match well with complete-basis-set results, compared to the finite-element inverse DFT results of Kanungo et al.^{22,30} At the same time, however, quantitative accuracy of reproducing the FCI densities using moderately-sized Slater basis sets was also moderate, with L_1 errors on the order of 10^{-3} per electron. At the time of this work, Slater atomic orbital basis

sets do not extend beyond quadruple zeta in quality, hindering progress towards more accurate densities via SlaterRKS. Future work to build larger, more complete Slater basis sets is likely to be instrumental in improving the accuracy of this method.

We anticipate that the SlaterRKS approach will be useful in providing facile analysis of strongly correlated molecules and their exchange-correlation potentials, using highly accurate reference wavefunctions (FCI) expressed in finite basis sets. The relative ease in convergence, physical behavior of the potentials, and correct asymptotics in the density are key advantages of SlaterRKS that merit further consideration of this method.

VI. ACKNOWLEDGEMENTS

This project has been supported by the Department of Energy through the grant DE-SC0022241. The authors acknowledge the computing time on the Perlmutter Supercomputer from the National Energy Research Scientific Computing Center (NERSC) through allocation m4067. ST thanks support by the Eric and Wendy Schmidt AI in Science Postdoctoral Fellowship, a Schmidt Futures program.

VII. REFERENCES

- ¹N. Mardirossian and M. Head-Gordon, “Thirty years of density functional theory in computational chemistry: an overview and extensive assessment of 200 density functionals,” *Mol. Phys.* **115**, 2315–2372 (2017).
- ²A. D. Becke, “Perspective: Fifty years of density-functional theory in chemical physics,” *J. Chem. Phys.* **140**, 18A301 (2014).
- ³K. Burke and L. O. Wagner, “DFT in a nutshell,” *Int. J. Quantum Chem.* **113**, 96–101 (2013).
- ⁴P. Hohenberg and W. Kohn, “Inhomogeneous electron gas,” *Phys. Rev.* **136**, B864–B871 (1964).
- ⁵W. Kohn and L. J. Sham, “Self-consistent equations including exchange and correlation effects,” *Phys. Rev.* **140**, A1133–A1138 (1965).
- ⁶J. P. Perdew, A. Ruzsinszky, J. Tao, V. N. Staroverov, G. E. Scuseria, and G. I. Csonka, “Prescription for the design and selection of density functional approximations: More constraint satisfaction with fewer fits,” *J. Chem. Phys.* **123**, 062201 (2005).
- ⁷A. J. Cohen and N. C. Handy, “Assessment of exchange correlation functionals,” *Chem. Phys. Lett.* **316**, 160–166 (2000).
- ⁸S. Kümmel and L. Kronik, “Orbital-dependent density functionals: Theory and applications,” *Rev. Mod. Phys.* **80**, 3–60 (2008).
- ⁹J. Sun, R. C. Remsing, Y. Zhang, Z. Sun, A. Ruzsinszky, H. Peng, Z. Yang, A. Paul, U. Waghmare, X. Wu, M. L. Klein, and J. P. Perdew, “Accurate first-principles structures and energies of diversely bonded systems from an efficient density functional,” *Nat. Chem.* **8**, 831–836 (2016).
- ¹⁰R. A. DiStasio, B. Santra, Z. Li, X. Wu, and R. Car, “The individual and collective effects of exact exchange and dispersion interactions on the ab initio structure of liquid water,” *J. Chem. Phys.* **141**, 084502 (2014).
- ¹¹M. Marsman, J. Paier, A. Stroppa, and G. Kresse, “Hybrid functionals applied to extended systems,” *J. Phys.: Condens. Matter* **20**, 064201 (2008).
- ¹²E. B. Isaacs and C. Wolverton, “Performance of the strongly constrained and appropriately normed density functional for solid-state materials,” *Phys. Rev. Materials* **2**, 063801 (2018).
- ¹³A. J. Cohen, P. Mori-Sánchez, and W. Yang, “Challenges for Density Functional Theory,” *Chem. Rev.* **112**, 289–320 (2012).
- ¹⁴P. Verma and D. G. Truhlar, “Status and Challenges of Density Functional Theory,” *Trends Chem.* **2**, 302–318 (2020).
- ¹⁵S. Crisostomo, R. Pederson, J. Kozłowski, B. Kalita, A. C. Cancio, K. Datchev, A. Wasserman, S. Song, and K. Burke, “Seven Useful Questions in Density Functional Theory,” (2022), arXiv:2207.05794 [math-ph, physics:quant-ph].
- ¹⁶K. R. Bryenton, A. A. Adeleke, S. G. Dale, and E. R. Johnson, “Delocalization error: The greatest outstanding challenge in density-functional theory,” *WIREs Comput Mol Sci.*, e1631 (2022).
- ¹⁷W. H. Green, D. J. Tozer, and N. C. Handy, “Learnings from exchange-correlation potentials,” *Chem. Phys. Lett.* **290**, 465–472 (1998).
- ¹⁸D. J. Tozer and N. C. Handy, “The development of new exchange-correlation functionals,” *J. Chem. Phys.* **108**, 2545–2555 (1998).
- ¹⁹P. J. Wilson, T. J. Bradley, and D. J. Tozer, “Hybrid exchange-correlation functional determined from thermochemical data and ab initio potentials,” *J. Chem. Phys.* **115**, 9233–9242 (2001).
- ²⁰G. Menconi, P. J. Wilson, and D. J. Tozer, “Emphasizing the exchange-correlation potential in functional development,” *J. Chem. Phys.* **114**, 3958–3967 (2001).
- ²¹A. P. Gaiduk, D. Mizzi, and V. N. Staroverov, “Self-interaction correction scheme for approximate Kohn-Sham potentials,” *Phys. Rev. A* **86**, 052518 (2012).
- ²²B. Kanungo, P. M. Zimmerman, and V. Gavini, “A Comparison of Exact and Model Exchange–Correlation Potentials for Molecules,” *J. Phys. Chem. Lett.* **12**, 12012–12019 (2021).
- ²³Y. Shi and A. Wasserman, “Inverse Kohn–Sham Density Functional Theory: Progress and Challenges,” *J. Phys. Chem. Lett.* **12**, 5308–5318 (2021).
- ²⁴E. Runge and E. K. U. Gross, “Density-Functional Theory for Time-Dependent Systems,” *Phys. Rev. Lett.* **52**, 997–1000 (1984).
- ²⁵W. Kohn, “ v -Representability and Density Functional Theory,” *Phys. Rev. Lett.* **51**, 1596–1598 (1983).
- ²⁶J. Hadamard, “Sur les Problèmes aux Dérivées Partielles et Leur Signification Physique,” *Princeton University Bulletin*, 49–52 (1902).
- ²⁷J. E. Harriman, “Densities, operators, and basis sets,” *Phys. Rev. A* **34**, 29–39 (1986).
- ²⁸J. E. Harriman, “Density and Density Matrices in Density Functional Theory,” in *Advances in Quantum Chemistry*, Density Functional Theory of Many-Fermion Systems, Vol. 21 (Academic Press, 1990) pp. 27–46.
- ²⁹V. N. Staroverov, G. E. Scuseria, and E. R. Davidson, “Optimized effective potentials yielding Hartree–Fock energies and densities,” *J. Chem. Phys.* **124**, 141103 (2006).
- ³⁰B. Kanungo, P. M. Zimmerman, and V. Gavini, “Exact exchange-correlation potentials from ground-state electron densities,” *Nat. Commun.* **10**, 4497 (2019).
- ³¹J. B. Stückrath and F. A. Bischoff, “Reduction of Hartree–Fock Wavefunctions to Kohn–Sham Effective Potentials Using Multiresolution Analysis,” *J. Chem. Theory Comput.* **17**, 1408–1420 (2021).
- ³²I. G. Ryabinkin, S. V. Kohut, and V. N. Staroverov, “Reduction of Electronic Wave Functions to Kohn-Sham Effective Potentials,” *Phys. Rev. Lett.* **115**, 083001 (2015).
- ³³R. Cuevas-Saavedra, P. W. Ayers, and V. N. Staroverov, “Kohn-sham exchange-correlation potentials from second-order reduced density matrices,” *J. Chem. Phys.* **143**, 244116 (2015).
- ³⁴A. Kumar, R. Singh, and M. K. Harbola, “Accurate effective potential for density amplitude and the corresponding Kohn–Sham exchange–correlation potential calculated from approximate wavefunctions,” *J. Phys. B: At. Mol. Opt. Phys.* **53**, 165002 (2020).
- ³⁵P. R. T. Schipper, O. V. Gritsenko, and E. J. Baerends, “Kohn-Sham potentials corresponding to Slater and Gaussian basis set densities,” *Theor. Chem. Acc.* **98**, 16–24 (1997).
- ³⁶T. Kato, “On the eigenfunctions of many-particle systems in quantum mechanics,” *Commun. Pure Appl. Math.* **10**, 151–177 (1957).
- ³⁷T. Helgaker, P. Jørgensen, and J. Olsen, *Molecular Electronic Structure Theory* (John Wiley & Sons, Ltd, Chichester, UK, 2000).
- ³⁸P. Reinhardt and P. E. Hoggan, “Cusps and derivatives for wave-functions expanded in Slater orbitals: A density study,” *Int. J. Quantum Chem.* **109**, 3191–3198 (2009).
- ³⁹D.-K. Dang, L. W. Wilson, and P. M. Zimmerman, “The numerical evaluation of Slater integrals on graphics processing units,” *J. Comput. Chem.* **43**, 1680–1689 (2022).
- ⁴⁰N. C. Handy, “The molecular physics lecture 2004: (i) Density functional theory, (ii) Quantum Monte Carlo,” *Mol. Phys.* **102**, 2399–2409 (2004).

- ⁴¹J. C. Slater, "A Generalized Self-Consistent Field Method," *Phys. Rev.* **91**, 528–530 (1953).
- ⁴²E. Ospadov, I. G. Ryabinkin, and V. N. Staroverov, "Improved method for generating exchange-correlation potentials from electronic wave functions," *J. Chem. Phys.* **146**, 084103 (2017).
- ⁴³B. I. Dunlap, J. W. D. Connolly, and J. R. Sabin, "On some approximations in applications of $X\alpha$ theory," *J. Chem. Phys.* **71**, 3396–3402 (1979).
- ⁴⁴H.-J. Werner, F. R. Manby, and P. J. Knowles, "Fast linear scaling second-order Møller-Plesset perturbation theory (MP2) using local and density fitting approximations," *J. Chem. Phys.* **118**, 8149–8160 (2003).
- ⁴⁵R. A. Distasio Jr., R. P. Steele, Y. M. Rhee, Y. Shao, and M. Head-Gordon, "An improved algorithm for analytical gradient evaluation in resolution-of-the-identity second-order Møller-Plesset perturbation theory: Application to alanine tetrapeptide conformational analysis," *J. Comput. Chem.* **28**, 839–856 (2007).
- ⁴⁶A. A. Holmes, N. M. Tubman, and C. J. Umrigar, "Heat-Bath Configuration Interaction: An Efficient Selected Configuration Interaction Algorithm Inspired by Heat-Bath Sampling," *J. Chem. Theory Comput.* **12**, 3674–3680 (2016).
- ⁴⁷S. Sharma, A. A. Holmes, G. Jeanmairet, A. Alavi, and C. J. Umrigar, "Semistochastic Heat-Bath Configuration Interaction Method: Selected Configuration Interaction with Semistochastic Perturbation Theory," *J. Chem. Theory Comput.* **13**, 1595–1604 (2017).
- ⁴⁸J. Li, M. Otten, A. A. Holmes, S. Sharma, and C. J. Umrigar, "Fast semistochastic heat-bath configuration interaction," *J. Chem. Phys.* **149**, 214110 (2018).
- ⁴⁹D.-K. Dang, J. A. Kammeraad, and P. M. Zimmerman, "Advances in Parallel Heat Bath Configuration Interaction," *J. Phys. Chem. A* **127**, 400–411 (2023).
- ⁵⁰A. D. Chien, A. A. Holmes, M. Otten, C. J. Umrigar, S. Sharma, and P. M. Zimmerman, "Excited States of Methylene, Polyenes, and Ozone from Heat-Bath Configuration Interaction," *J. Phys. Chem. A* **122**, 2714–2722 (2018).
- ⁵¹E. Van Lenthe and E. J. Baerends, "Optimized Slater-type basis sets for the elements 1–118," *J. Comput. Chem.* **24**, 1142–1156 (2003).
- ⁵²D. P. Chong, E. Van Lenthe, S. Van Gisbergen, and E. J. Baerends, "Even-tempered slater-type orbitals revisited: From hydrogen to krypton," *Journal of Computational Chemistry* **25**, 1030–1036 (2004).
- ⁵³R. D. Johnson, "Nist 101. computational chemistry comparison and benchmark database," (1999).
- ⁵⁴A. D. Becke, "A multicenter numerical integration scheme for polyatomic molecules," *J. Chem. Phys.* **88**, 2547–2553 (1988).
- ⁵⁵M. E. Mura and P. J. Knowles, "Improved radial grids for quadrature in molecular density-functional calculations," *J. Chem. Phys.* **104**, 9848–9858 (1996).
- ⁵⁶C. W. Murray, N. C. Handy, and G. J. Laming, "Quadrature schemes for integrals of density functional theory," *Mol. Phys.* **78**, 997–1014 (1993).
- ⁵⁷V. I. Lebedev, "Quadratures on a sphere," *USSR Computational Mathematics and Mathematical Physics* **16**, 10–24 (1976).
- ⁵⁸T. Schmidt, E. Kraisler, L. Kronik, and S. Kümmel, "One-electron self-interaction and the asymptotics of the Kohn–Sham potential: an impaired relation," *Phys. Chem. Chem. Phys.* **16**, 14357–14367 (2014).
- ⁵⁹Q. Wu, P. W. Ayers, and W. Yang, "Density-functional theory calculations with correct long-range potentials," *J. Chem. Phys.* **119**, 2978 (2003).
- ⁶⁰V. N. Staroverov, G. E. Scuseria, J. Tao, and J. P. Perdew, "Tests of a ladder of density functionals for bulk solids and surfaces," *Phys. Rev. B* **69**, 075102 (2004).
- ⁶¹E. Kraisler, "Asymptotic Behavior of the Exchange-Correlation Energy Density and the Kohn-Sham Potential in Density Functional Theory: Exact Results and Strategy for Approximations," *Isr. J. Chem.* **60**, 805–822 (2020).
- ⁶²C. D. Sherrill, M. L. Leininger, T. J. Van Huis, and H. F. Schaefer, "Structures and vibrational frequencies in the full configuration interaction limit: Predictions for four electronic states of methylene using a triple-zeta plus double polarization (TZ2P) basis," *J. Chem. Phys.* **108**, 1040–1049 (1998).
- ⁶³P. M. Zimmerman, J. Toulouse, Z. Zhang, C. B. Musgrave, and C. J. Umrigar, "Excited states of methylene from quantum Monte Carlo," *J. Chem. Phys.* **131**, 124103 (2009).
- ⁶⁴R. C. Morrison and Q. Zhao, "Solution to the Kohn-Sham equations using reference densities from accurate, correlated wave functions for the neutral atoms helium through argon," *Phys. Rev. A* **51**, 1980–1984 (1995).
- ⁶⁵P. R. T. Schipper, O. V. Gritsenko, and E. J. Baerends, "One - determinantal pure state versus ensemble Kohn-Sham solutions in the case of strong electron correlation: CH₂ and C₂," *Theor. Chem. Acc.* **99**, 329–343 (1998).
- ⁶⁶O. V. Gritsenko, R. v. Leeuwen, and E. J. Baerends, "Molecular exchange-correlation Kohn–Sham potential and energy density from ab initio first- and second-order density matrices: Examples for XH (X=Li, B, F)," *J. Chem. Phys.* **104**, 8535–8545 (1996).